2018 IEEE 14th International Conference on Control and Automation (ICCA)
June 12-15, 2018. Anchorage, Alaska, USA

Model Predictive Control for MicroCSP Integration into a Building HVAC System

Mohamed Toub*, Chethan R. Reddy†, Meysam Razmara†, Mahdi Shahbakhti†, Rush D. Robinett III†, and Ghassane Aniba*
*Mohammadia School of Engineering, Mohammed V University of Rabat, Rabat, Morocco
Emails: mohamedtoub@research.emi.ac.ma, ghassane@emi.ac.ma

†Michigan Technological University, Houghton, MI, USA
Emails: {creddy, mrazmara, mahdish, rdrobine}@mtu.edu

***Abstract*—Micro-scale concentrated solar power (MicroCSP) is a promising technology that uses solar energy to provide electrical energy and thermal energy for use in buildings. This paper presents a model predictive control (MPC) framework to minimize the energy consumption of the building heating, ventilation, and air-conditioning (HVAC) system by integrating it with a microCSP. To this end, a microCSP model is developed and then integrated to the building model of an office building in Michigan Technological University. The designed MPC framework optimizes thermal energy storage (TES) usage and thermal energy flows from the heat pumps to the building rooms. The optimal control results show that the integration of microCSP to the building HVAC system reduces the HVAC energy consumption by almost half (47-52%) by optimally utilizing the solar energy. The designed MPC framework provides 46% energy saving, compared to a heuristically designed rule-based controller for the combined HVAC and microCSP systems.**

I. Introduction

According to the United States Environmental Protection Agency (EPA) [1], in 2015, 34% of the total CO2 emissions in the US was caused by electricity generation. Residential and commercial buildings accounted for 34% and 37% of total electricity consumption in the US in 2017, respectively [2]. Thirty percent of the energy consumption in buildings in the US in 2017 was found to be due to the heating, ventilation, and air-conditioning (HVAC) systems [3]. Hence, the considerable amount of energy consumption and associated CO2 emissions from HVAC systems makes them a good candidate for energy efficiency programs.

CSP plants have been utilized over the past four decades; however, micro-scale concentrated solar power (MicroCSP) systems with power less than 1 MW have become more popular in recent years [4]. One of the well-known technologies in microCSP is the use of organic rankine cycles (ORC) to convert low-grade thermal energy into electrical energy [5].

MicroCSP is a promising technology for use in buildings and HVAC systems, particularly for heating purposes. In the microCSP plant in this study, solar energy absorbed by the PTC is converted to thermal energy. This thermal energy is stored in a TES so that it can be dispatched to the ORC when needed. The ORC produces electricity and cogenerated low-grade heat. This low-grade heat is used to preheat the fresh air coming from the Energy Recovery Ventilator (ERV) and/or the recycled air from the rooms in the building. In addition, electrical energy contribution of the ORC reduces the electrical energy from the grid.

Control of the microCSP system when integrated to the building HVAC system is challenging. Solar irradiation is limited to daylight hours; thus, for optimal usage of energy from microCSP, TES has to store the thermal energy from PTC and dispatch it to the ORC according to the building HVAC demand. The controller has to optimally decide when to dispatch thermal energy from TES to ORC, using solar energy, and when to operate the room heat pump, using electrical energy from the grid.

Model predictive controllers (MPC) have been successfully used for control of building HVAC systems with heat pumps [6], PV panels and batteries [7]. MPC can provide real time optimal solution and can handle constraints on TES state of charge, heat pump operating limits, and meet comfort bounds in the building thermal zones. Hence in this study, we develop models of the building and microCSP, and design MPC to optimally control TES usage along with the thermal energy flows from the heat pumps to the building. MPC controls the room temperature based on the current and future room temperature set points and solar irradiation forecast.

This paper presents our first results for showing energy saving potential by optimal use of a microCSP system for building HVAC systems. The building model and HVAC model are based on a real test setup at Michigan Technological University [8] and the microCSP model is based on our recently purchased system [9].

To the best of authors knowledge, this paper presents the first study undertaken for real-time model-based predictive control (MPC) for the optimal integration of microCSP into a building HVAC system.

This work is supported in part by the US National Science Foundation (Grant #1541148), the Richard and Elizabeth Henes Professorship of Mechanical Engineering at Michigan Technological University, and the Institute for Research on Solar and New Energies (IRESEN) in Morocco (reference: InnoTherm-13-MicroCSP).

II. Building Testbed

The building testbed considered in this work is the Lakeshore Center building at Michigan Technological University. This three-story office building has an area of 61,500 ft^2 where each room or office has its individual heat pump for heating purposes. This building is equipped with a Ground Source Heat-Pump (GSHP) that supplies geothermal energy from the ground to the individual heat-pumps in the rooms; however, in this study, we assume that the GSHP is replaced with a microCSP testbed that will supply cogenerated low-grade heat to the rooms' heat-pumps. In the microCSP, solar energy is converted to thermal energy by the PTC ($\dot{Q}_{SOL}$) and stored in the TES. This stored thermal energy is delivered to the ORC ($\dot{Q}_{TES}$), which cogenerates electrical power (P_{ORC}) and thermal power ($\dot{Q}_{COG}$) as shown in Fig. 1.

Each room is considered as an individual thermal zone in the testbed and is equipped with a thermocouple with $\pm 0.2°$C accuracy. The temperature data is recorded with 1-minute sampling time.

III. Modeling

A. PTC Model

The solar field considered in this paper is composed of two rows of PTC PTMx-24 from Soltigua [10]. A tracking system allows the collectors to track the sun from east to west around a horizontal north-south axis. Equation (1) shows the relationship between the declination angle (δ), the zenith angle (θ_z), the hour angle (ω), and the incidence angle (θ) which is the angle between the solar beam and the line normal to the tracking plane [11].

$$\cos(\theta) = \sqrt{\cos^2(\delta) \times \cos^2(\omega) + \cos^2(\theta_z)} \quad (1)$$

The declination angle is the angle between the position of the sun at noon, and the plane of the equator. This angle varies throughout the year $-23.45° \leq \delta \leq 23.45°$. The following equation is used to calculate δ [12]:

$$\delta = 23.45 \times \sin(\frac{281 + n}{365} \times 2\pi) \quad (2)$$

where, n is the day number starting from January 1^{st}.

The hour angle (ω) is the angle between the sun and the local meridian such as

$$\omega = (T_{Solar} - 12) \times \frac{2\pi}{24} \quad (3)$$

where, T_{Solar} is the solar time. The solar time is related to the standard time $T_{Standard}$ by the following relationship

$$T_{Solar} = T_{Standard} - DST + \frac{L_{st} - L_{loc}}{15} + \frac{E_t}{60} \quad (4)$$

where, DST is the Daylight Saving Time ($DST = 1$ during daylight saving time and 0 otherwise), L_{st} and L_{loc} are the meridians for the local time zone and the collector site, respectively. E_t is the well-known equation of time, that takes into consideration the elliptical shape of the earth's orbit [13].

The zenith angle δ_z is the angle between the zenith, the line normal to the ground, and the sun. It is related to the declination angle δ, the hour angle ω, and the latitude angle ϕ as follows [12]:

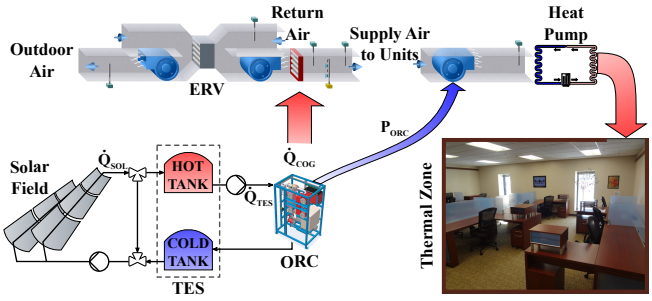

Fig. 1. Building HVAC and microCSP setup in this study.

$$\cos(\theta_z) = \cos(\delta) \times \cos(\omega) \times \cos(\phi) + \sin(\delta) \times \sin(\phi) \quad (5)$$

After finding the incidence angle, the solar power absorbed by the collectors is calculated by

$$\dot{Q}_{gain} = \eta_o \times IAM \times \cos(\theta) \times A_p \times DNI \quad (6)$$

where, DNI is the direct normal irradiation, A_p is the aperture area, $\eta_o = 0.748$ is the collectors' optical efficiency specified by the manufacturer [10], and IAM is the incident angle modifier that correlates the losses related to the imperfection of the reflectors.

Equation (7) is a correlation used to predict the heat loss in the collectors [14]:

$$\dot{Q}_{loss} = a_1 \times \frac{(T_{htf} - T_{amb})}{DNI} \quad (7)$$

where, $a_1 = 0.64$ is the heat loss coefficient given by the collectors manufacturer [10], and T_{amb} is the ambient temperature. Assuming that the heat transfer fluid (HTF) temperature is linear along the collectors, we consider T_{htf} as the average temperature of the HTF in the collectors.

$$T_{htf} = \frac{T_{htf,in} + T_{htf,out}}{2} \quad (8)$$

Where, $T_{htf,in}$ and $T_{htf,out}$ are the HTF inlet and outlet temperatures of the solar field, respectively.

Finally, the heat power produced by the solar field is

$$\dot{Q}_{SOL} = \dot{Q}_{gain} - \dot{Q}_{loss} \quad (9)$$

It should be noted that the mass flow rate of the HTF ($\dot{m}_{htf}$) is controlled to increase the HTF temperature in the solar field by $\Delta T = 40°C$ (i.e., $T_{htf,in} = 140°C$, $T_{htf,out} = 180°C$).

The collector model was validated using experimental data from the manufacturer Soltigua for the PTMx-24 [15].

B. TES Model

In this paper, the TES system can store the energy from the solar field so that it can be used when there is a demand for thermal and electrical energy by the building. In general, TES is being used to mitigate intermittent power generation and ensure reliable and uninterruptible power supply through ORC in the event of temporary weather changes. For our study a two-tank direct system is considered as the TES (Fig. 1). Both tanks are modeled as a fully-mixed cylindrical

tank with a constant cross-sectional area that contains a variable quantity of the HTF and have the capacity to store the whole volume of HTF. During charging, the hot tank accumulates the high-temperature HTF produced by the solar field, while the cold tank sends back the low-temperature HTF to the solar field. During discharging, the hot tank supplies the high-temperature HTF to the power cycle which uses the HTF thermal energy to produce electricity and low-grade heat and directs the low-temperature HTF to the cold tank.

The state of charge (SOC) of the TES is calculated using the following equation.

$$\dot{SOC} = \frac{(\dot{Q}_{SOL} - \dot{Q}_{TES})}{C_{TES}} \tag{10}$$

Where, $\dot{Q}_{SOL}$ is the solar field generation, $\dot{Q}_{TES}$ is the power from the TES to the ORC, and C_{TES} is the TES capacity.

C. ORC Model

This work uses the ORC system ENO-10LT manufactured by ENOGIA [9]. This system is a low-temperature 10 kW ORC module, which uses R245fa as the working fluid (WF).

In the ORC, the WF enters the turbine in a vapor state at high pressure and high temperature (State 1). The high pressure fluid energy is converted to mechanical energy in turbine and then converted to electrical energy in the power generator. After passing the turbine blades, the WF remains at its vapor state at a lower temperature and pressure (State 2). Then, the WF enters the condenser where its state changes to liquid and thereby rejecting heat through the heat exchanger (State 3). This heat will be used to heat the fresh air coming from the ERV and/or the recycled air from the rooms. The low temperature and low pressure liquid is then compressed by a pump (driven by a motor) to increase its pressure (State 4). The cycle is repeated when the WF passes through the evaporator and acquires heat extracted from the HTF coming from the TES, which changes the state to vapor and increases its temperature.

Using the First Law of Thermodynamics for the ORC as a closed system yields:

$$P_{gross} = \eta_{gen} \times \dot{m}_{WF} \times (h_1 - h_2) \tag{11a}$$

$$P_{motor} = \frac{\dot{m}_{WF} \times (h_4 - h_3)}{\eta_{motor}} \tag{11b}$$

$$P_{ORC} = P_{gross} - P_{motor} \tag{11c}$$

$$\dot{Q}_{COG} = \dot{m}_{WF} \times (h_2 - h_3) \tag{11d}$$

$$\dot{Q}_{TES} = \dot{m}_{tes} \times c_{p,htf} \times (T_{ev,in} - T_{ev,out}) \tag{11e}$$

where, P_{gross} is the gross electrical power generated by the turbine, P_{motor} is the electrical power consumed by the motor, P_{ORC} is the net electrical power generated by the ORC, $\dot{Q}_{COG}$ is the cogeneration heat rate delivered by the ORC, $\dot{Q}_{TES}$ is the heat rate from the HTF to the ORC evaporator, η_{gen} and η_{motor} are the efficiencies of the ORC turbine generator and motor, respectively. $\dot{m}_{tes}$ is the HTF mass flow rate from the TES, $T_{ev,in}$ and $T_{ev,out}$ are the HTF inlet and outlet temperatures to the ORC evaporator, respectively.

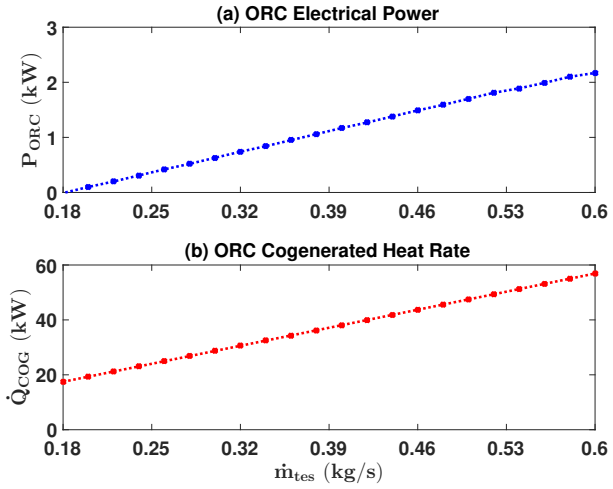

Fig. 2. ORC electric power (P_{ORC}) and cogeneration heat production rate ($\dot{Q}_{COG}$) as a function of HTF mass flow rate ($\dot{m}_{htf}$)

It can be shown that

$$P_{ORC} = f(\dot{m}_{WF}, \dot{m}_{tes}, c_{p,htf}, T_{ev,in}, T_{ev,out}, h_3, r_p, \eta_{gen}, \eta_{motor}) \tag{12a}$$

$$\dot{Q}_{COG} = g(\dot{m}_{WF}, \dot{m}_{tes}, c_{p,htf}, T_{ev,in}, T_{ev,out}, h_3, r_p, \eta_{gen}, \eta_{motor}) \tag{12b}$$

where, r_p is the turbine pressure ratio of the ORC.

In Equation (12), $\dot{m}_{WF}$ is kept constant in the ORC module in this study; $T_{ev,in}$ and $T_{ev,out}$ are constant design temperatures, $c_{p,htf}$ is considered constant. h_3 is a function of T_3 and P_3 which are the condensation temperature and pressure, that are kept constant by controlling the coolant mass flow rate. η_{gen}, and η_{motor} are constant for the given system. The r_p is variable according to the power needed and is fixed to a nominal value of 3 to increase efficiency in the ORC working range. Thus, P_{ORC} and $\dot{Q}_{COG}$ are functions of $\dot{m}_{tes}$ for the ORC system in this study. The variation of P_{ORC} and $\dot{Q}_{COG}$ as a function of $\dot{m}_{tes}$ is shown in Fig. 2. The mathematical model in this work was validated against experimental data [16] from the manufacturer and the errors for estimating P_{ORC} and $\dot{Q}_{COG}$ were less than 10%.

D. Building Thermal Model and HVAC Power Consumption

The building testbed presented in section II (i.e., Lakeshore Center at Michigan Technological University) is modeled by using the well-known RC modeling approach where heat storage and heat transfer between adjacent zones and outdoor are modeled with capacitive, resistive, and current elements. The details of the building testbed modeling and experimental validation are found in our previous works in [8], [17], [18].

The building HVAC energy consumption is represented by the energy index ($I_{e,t}$) which is calculated as follows

$$I_{e,t} = \sum_{t=0}^{t_f} \sum_{i=1}^{N_z} \left(P_{i,t}^{F} + P_{i,t}^{H}\right) \tag{13}$$

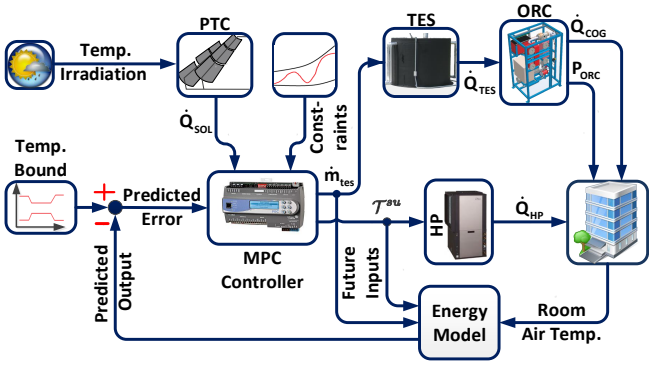

Fig. 3. Schematic of the designed MPC for optimal energy control of the combined microCSP and building HVAC system.

where, N_z is the number of building thermal zones. Since this work concentrates on the heating mode, the power consumed by the building HVAC system is the sum of the ventilation fan power ($P^F_{i,t}$) and the heat pumps (HPs) power consumption ($P^H_{i,t}$). The HVAC electrical power consumption is calculated by:

$$P^F_{i,t} = \gamma_F \times (\dot{m}^r_{i,t})^3 \tag{14a}$$

$$P^H_{i,t} = \frac{\dot{m}^r_{i,t} \times c_{p,air} \times (\mathcal{T}^{su}_{i,t} - T^{HP}_{i,t})}{COP} \tag{14b}$$

where, γ_F is power coefficient of the fan and $\dot{m}^r_i$ is the mass flow rate of the supply air. Equation (14b) calculates the power consumption of the HPs as a function of the supply air temperature ($\mathcal{T}^{su}$), the HPs inlet temperatures ($T^{HP}_{i,t}$), and the Coefficient of Performance (COP) of the HPs. The HPs inlet temperature is calculated by Equation (15a) and (15b) for occupancy and non-occupancy modes, respectively, according to the ANSI/ASHRAE Standard 62.1-2007 for required indoor air quality.

$$T^{HP}_{i,t} = \frac{\dot{m}^r_{i,t} - \dot{m}^v_{i,t}}{\dot{m}^r_{i,t}} \times T^r_{i,t} + \frac{\dot{m}^v_{i,t}}{\dot{m}^r_{i,t}} \times T^{ERV}_t + \frac{\dot{Q}_{COG,t}}{N_z \times \dot{m}^r_{i,t} \times c_{p,air}} \tag{15a}$$

$$T^{HP}_{i,t} = T^r_{i,t} + \frac{\dot{Q}_{COG,t}}{N_z \times \dot{m}^r_{i,t} \times c_{p,air}} \tag{15b}$$

The ERV outlet temperature is calculated using the Energy Recovery Effectiveness (ERE) defined by ASHRAE Standard 84 and AHRI Standard 1060:

$$T^{ERV}_t = T_{amb,t} + ERE \times (T^r_{i,t} - T_{amb,t}) \tag{16}$$

IV. Building Model Predictive Control

Fig. 3 depicts the structure of our designed MPC for optimal energy control of the building with the microCSP system. To minimize the HVAC energy consumption of the building, the objective function is defined according to Equation (17) subject to the constraints listed in Equation (18). The optimization problem is solved at each time step t to find the N future values of the two inputs, including the supply air temperature ($\mathcal{T}^{su}$) and the HTF mass flow rate form the TES ($\dot{m}_{tes}$). Here, room temperature soft constraints are used to guarantee feasibility of optimal solution at all times. The MPC optimization model inputs are weather forecast and irradiation. Room air temperature bounds are defined according to ANSI/ASHRAE Standard 55-2013, and

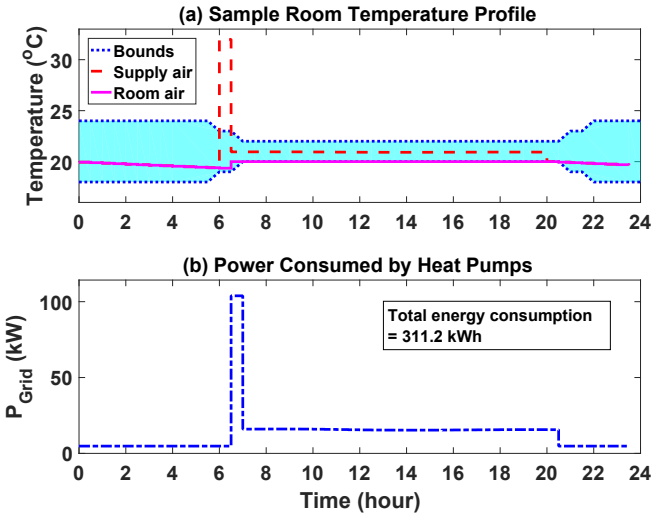

Fig. 4. Optimal HVAC control for a sample room in the building without microCSP system: (a) supply air temperature and resulting room air temperature, and (b) power consumed in the building supplied by the grid (P_{Grid}).

ventilation requirements are set based on ANSI/ASHRAE Standard 62.1-2007.

$$\min_{\dot{m}_{tes},\mathcal{T}^{su},\bar{\epsilon},\underline{\epsilon}} \{(I_{e,t} - \overbrace{\sum_{t=0}^{t_f} P_{ORC,t} \times \Delta t}^{P_{Grid,t} \times \Delta t}) + \rho \times (|\bar{\epsilon}|_1 + |\underline{\epsilon}|_1)\} \tag{17}$$

Subject to the following constraints:

$$T_{t+k+1|t} = A.T_{t+k|t} + B.\mathcal{T}^{su}_{t+k|t} + Ed_{t+k|t} \tag{18a}$$

$$T^r_{t+k|t} = C.T_{t+k|t} \tag{18b}$$

$$P_{ORC,t+k|t} = f(\dot{m}_{tes_{t+k|t}}) \tag{18c}$$

$$\dot{Q}_{COG,t+k|t} = g(\dot{m}_{tes_{t+k|t}}) \tag{18d}$$

$$SOC_{t+k+1|t} = SOC_{t+k|t} + \frac{(\dot{Q}_{SOL_{t+k|t}} - \dot{Q}_{TES_{t+k|t}}) \times \Delta t}{C_{TES}} \tag{18e}$$

$$\underline{SOC} \leq SOC_{t+k+1|t} \leq \overline{SOC} \tag{18f}$$

$$0 \leq \dot{m}_{tes_{t+k|t}} \leq \dot{m}_{max} \tag{18g}$$

$$T^{HP}_{t+k|t} \leq \mathcal{T}^{su}_{t+k|t} \leq \bar{T}_{t+k|t} \tag{18h}$$

$$\underline{T}^r_{t+k|t} - \underline{\epsilon}_{t+k|t} \leq T^r_{t+k|t} \leq \bar{T}^r_{t+k|t} + \bar{\epsilon}_{t+k|t} \tag{18i}$$

$$\underline{\epsilon}_{t+k|t}, \bar{\epsilon}_{t+k|t} \geq 0 \tag{18j}$$

Equations (18a) and (18b) represent the buildings state-space model; (18c) and (18d) constitute the ORC model; (18e) includes the TES model for calculating SOC; (18f) shows the TES lower bound $\underline{SOC}$ and upper bound $\overline{SOC}$ set to 5% and 95%, respectively; (18g) shows the ORC evaporator mass flow limit ($\dot{m}_{max}$) set by the manufacturer [9]; (18h) is the supply air temperature constraint based on HP settings; (18i) is the output constraint on room air temperature; finally, (18j) includes the slack variables constraints.

V. Control Results

The building, solar field, and TES models are implemented in MATLAB®. For optimization problem formula-

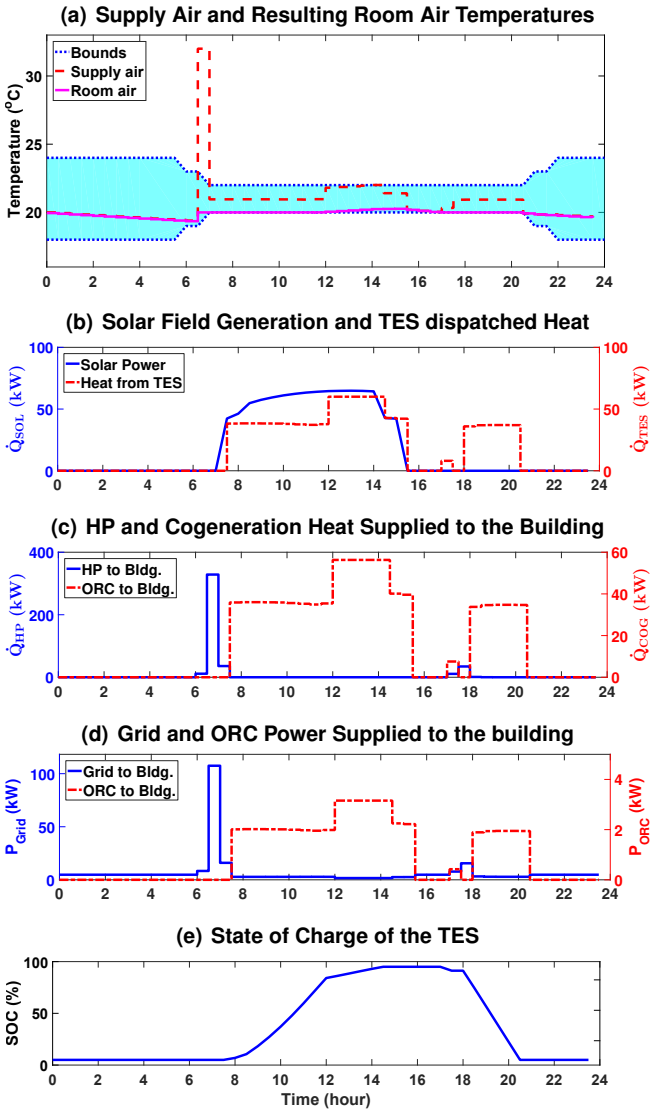

Fig. 5. MPC results with microCSP integration into the building.

tion, YALMIP Toolbox [19] was used in MATLAB® which provides a symbolic syntax to interface with the solver.

The building is simulated with 48 thermal zones. For MPC simulations, a prediction horizon of $N = 24$ with a time step of $\Delta t = 30$ minutes is used. The simulations are done for a winter day in Houghton, MI.

A. Optimal HVAC Control

This section presents the results of the building HVAC control without the microCSP system. The section is included mainly for comparing this work control results with those without utilizing the microCSP system. The MPC framework formulation is similar to that in Equations (17) and (18) excluding (18c), (18d), (18e), (18f), and (18g) which are related to the ORC and TES models and constraints. Details about the optimal HVAC control and the optimization problem formulation can be found in [17].

Fig. 4(a) shows the air temperature of a sample room. As seen from the figure, the room temperature is within the comfort temperature bounds. The only control variable is the supply air temperature ($\mathcal{T}^{su}$). The optimizer minimizes the energy consumption of the building HVAC system by supplying just enough heat to keep the room air temperature at the lower comfort bound, as shown in Fig. 4(a). Heating supply air is done by the heat pumps which take power from the grid. Since there is no other source of heat and only HVAC loads are considered, the power from the grid has the same profile of the supply air temperature (Fig. 4(b)).

B. Building Predictive Control with microCSP

The supply air temperature and the air temperature of a sample room within the comfort temperature bounds are shown in Fig. 5(a). It can be seen that, when the building is not occupied (i.e., from midnight to 6 AM), the heat pumps are shut down, while the room temperature is inside the bounds. Then, during the very early morning, just before the beginning of the occupancy mode, the optimizer turns on the heat pumps for preheating to ensure that the room temperature stays within the comfort temperature bounds. To minimize HVAC energy consumption of the building, the optimizer tries to keep the room air temperature at the lower comfort bound, during the occupancy mode, by supplying the minimum heat needed. Fig. 5(b) depicts the heat produced in the solar field, and the heat dispatched from the TES to the ORC. When there is no microCSP, all the heat required during the occupancy mode is supplied by the heat pumps (Fig. 4). Whereas with microCSP, the heat pumps supply the required heat only during the beginning of the occupancy mode until the TES is charged with enough heat from the solar field to run the ORC and supply cogenerated heat to the building (Fig. 5(c)). Fig. 5(d) shows the grid power supplied to the heat pumps when they are on, and the electricity produced by the ORC which is consumed by the ventilation fans. The excess of heat produced by the solar field and not used by the ORC is stored in the TES, causing the SOC of the TES to increase. The stored heat is recovered later, at the end of the day when there is not enough solar irradiation at the solar field to produce heat, and the SOC diminishes until it reaches its lower bound as it can be seen in Fig. 5(e).

Table I provides the energy consumption comparison for showing the effect of utilizing microCSP and design of MPC, compared to a Rule-Based Controller (RBC).

The RBC works as follows. To keep the room air temperature within the comfort bounds, at each time step the RBC for building HVAC with microCSP compares the room air temperature with a dead-band. Then the RBC turns the heat pumps on for the duration of Δt when the room air temperature goes beyond the dead-band.

TABLE I
ELECTRICAL ENERGY CONSUMPTION COMPARISON.

System	Control Type	Elec. Consumption [kWh/day]	Energy Saving* [%]
HVAC	MPC	311.2	0
HVAC + microCSP	RBC	293	6
HVAC + microCSP	MPC	157	49.6

*calculated by comparison with MPC based control of HVAC system.

Compared to the HVAC system without a microCSP, the integration of microCSP with an RBC results in 6% energy saving, while the designed MPC framework leads to 49.6% energy saving. The key point of this comparison is that an MPC framework needs to be designed to fully take advantage of the microCSP thermal and electrical energies for the integration into the building HVAC system.

C. Monte-Carlo Analysis

The results presented in Section V-B show important savings in the HVAC energy consumption of the building. However, prediction uncertainty in solar irradiation and outdoor temperatures were not taken into account. Hence, a probabilistic analysis using Monte-Carlo simulations is carried out to account for these uncertainties. These Monte-Carlo simulations can show possible outcomes for the energy savings and how likely each outcome is to happen.

To account for uncertainty prediction of solar irradiation and outdoor temperature, an additive uncertainty with a normal distribution is considered and random numbers are generated for each factor (i.e., irradiation and outdoor temperature) using the results from [20]. Fig. 6 presents the probability distribution of the energy saving. It is shown that the probability of at least 50% energy saving is around 75%. Furthermore, Fig. 6 shows that in the worst case, the energy saving will drop to 47%.

The Monte-Carlo analysis results show that the building MPC with microCSP guarantee important energy saving even with the presence of prediction uncertainty. It should be noted that all the results in Section V were completed for a sunny day in Houghton, MI in the United States. The energy saving percentages are anticipated to change for cloudy days or days with different outdoor temperatures.

VI. Summary & Conclusion

This paper presented the first study undertaken for real-time MPC for the optimal integration of microCSP into a building HVAC system. First, a control-oriented model was developed for a microCSP system integrated into a building HVAC system. Next, an MPC framework was designed to optimally coordinate thermal and electrical energy sources according to HVAC needs in the building. Finally, the results show that adding microCSP and utilizing a rule-based controller contributes to only 6% energy saving, while the designed MPC framework increases the energy saving to 49.6%, compared to the HVAC system without a microCSP system. Furthermore, Monte-Carlo simulation results show that the energy saving variations are within $\pm 3\%$ with the presence of prediction uncertainties on the solar irradiation and outdoor temperature.

Future work will investigate the electrical cost minimization of the building HVAC integrating a microCSP system compared to a PV system with batteries, using MPC control.

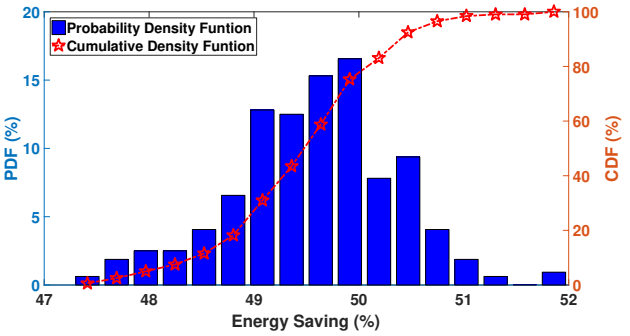

Fig. 6. Monte-Carlo simulation results showing probability of HVAC energy saving by applying MPC and utilizing microCSP, compared to HVAC control without microCSP using MPC framework.

References

[1] EPA, "Inventory of U.S. Greenhouse Gas Emissions and Sinks: 1990-2015," Apr. 2016, (Accessed on 18 January 2018). [Online]. Available: https://www.epa.gov/ghgemissions/inventory-us-greenhouse-gas-emissions-and-sinks-1990-2015

[2] EIA, "Electric power monthly with data for november 2017," Jan. 2018. [Online]. Available: https://www.eia.gov/electricity/monthly/current-month/epm.pdf

[3] ——, "International energy outlook 2017," (Accessed on 18 January 2018). [Online]. Available: https://www.eia.gov/outlooks/aeo/pdf/0383(2017).pdf

[4] A. Mueller, M. Orosz, A. K. Narasimhan, R. Kamal, H. F. Hemond, and Y. Goswami, "Evolution and feasibility of decentralized concentrating solar thermal power systems for modern energy access in rural areas," *MRS Energy & Sustainability-A Review Journal*, vol. 3, 2016.

[5] A. Giovannelli, "State of the art on small-scale concentrated solar power plants," *Energy Procedia*, vol. 82, pp. 607–614, 2015.

[6] M. Maasoumy and A. Sangiovanni-Vincentelli, "Total and peak energy consumption minimization of building HVAC systems using model predictive control," *IEEE Design Test of Computers*, vol. 29, no. 4, pp. 26–35, Aug 2012.

[7] M. Razmara, G. R. Bharati, D. Hanover, M. Shahbakhti, S. Paudyal, and R. D. Robinett, "Enabling demand response programs via predictive control of building-to-grid systems integrated with PV panels and energy storage systems," in *2017 American Control Conference (ACC)*, May 2017, pp. 56–61.

[8] M. Maasoumy, M. Razmara, M. Shahbakhti, and A. Sangiovanni-Vincentelli, "Selecting Building Predictive Control Based on Model Uncertainty," in *American Control Conference (ACC)*, 2014.

[9] ENOGIA SAS. (2017, Jun.) DATASHEET: ENOGIA'S ENO-10LT ORC SYSTEM FACT SHEET. [Online]. Available: http://www.enogia.com/images/offer/datasheet-ENO10LT.pdf

[10] "Soltigua - Parabolic Troughs PTMx," (Accessed on 27 August 2017). [Online]. Available: http://www.soltigua.com/ptmx-introduction/

[11] J. A. Duffie and W. A. Beckman, *Solar engineering of thermal processes*, ch. Solar Radiation.

[12] P. Cooper, "The absorption of radiation in solar stills," *Solar energy*, vol. 12, no. 3, pp. 333–346, 1969.

[13] J. Spencer, "Fourier series representation of the position of the sun," *Search*, vol. 2, no. 5, pp. 172–172, 1971.

[14] R. Forristall, "Heat transfer analysis and modeling of a parabolic trough solar receiver implemented in engineering equation solver," National Renewable Energy Lab., Golden, CO.(US), Tech. Rep., 2003.

[15] Agenzia Nazionale per le Nuove tecnologie, l'Energia e lo Sviluppo economico sostenibile (ENEA), "Performance test report summary according to EN 12975-2:2006," technical communication with SOLTIGUA, (Accessed on 22 March 2017).

[16] J. Drouineau, technical communication with ENOGIA.

[17] M. Razmara, M. Maasoumy, M. Shahbakhti, and R. D. Robinett III, "Optimal exergy control of building HVAC system," *J. Applied Energy*, vol. 156, pp. 555–565, 2015.

[18] M. Razmara, G. Bharati, M. Shahbakhti, S. Paudyal, and R. D. R. III, "Bilevel Optimization Framework for Smart Building-to-Grid Systems," *IEEE Transactions on Smart Grid*, no. 99, 2016.

[19] J. Lofberg, "YALMIP: A toolbox for modeling and optimization in MATLAB," in *2004 IEEE International Symposium on Computer Aided Control Systems Design*. IEEE, 2004, pp. 284–289.

[20] M. Razmara, G. Bharati, D. Hanover, M. Shahbakhti, S. Paudyal, and R. Robinett III, "Building-to-grid predictive power flow control for demand response and demand flexibility programs," *Applied Energy*, vol. 203, pp. 128–141, 2017.